

Article

Columbite–Tantalite from Northern Scandinavia (Kaustinen, Kolmozero) Pegmatites: An Optical and Spectroscopic Properties

Miłosz Huber ^{1,*} , Daniel Kamiński ² and Urszula Maciołek ² 

¹ Department of Geology, Soil Science and Geoinformacy, Faculty of Earth Science and Spatial Management, Maria Curie-Skłodowska University, 2d/107 Kraśnickie Rd, 20-718 Lublin, Poland

² Institute of Chemical Sciences, Faculty of Chemistry, Maria Curie-Skłodowska University in Lublin, 20-031 Lublin, Poland

* Correspondence: milosz.huber@mail.umcs.pl; Tel.: +48-69-228-35-72

Abstract: LCT (lithium–cesium–tantalum) pegmatites from the Kaustinen and Kolmozero regions contain columbite–tantalite mineralization, which has been presented in this study. Crystal structure, Raman microscopy, and optical property analyses of these minerals were performed. As a result of the structural studies and micro-area analyses, it was determined that these minerals in the pegmatites in question constitute a solid solution with numerous Mn-Fe and Nb-Ta substitutions within a single crystal. The ratio between Mn-Fe and Nb-Ta can change from crystal to crystal, which makes it impossible to find precise stoichiometry between these ions. The crystallization conditions of these minerals were also determined by studying the associations of other rock-forming minerals and accessory minerals in the discussed rocks.

Keywords: columbite; tantalite; optical properties; crystal structure; Kaustinen; Kolmozero



Citation: Huber, M.; Kamiński, D.; Maciołek, U. Columbite–Tantalite from Northern Scandinavia (Kaustinen, Kolmozero) Pegmatites: An Optical and Spectroscopic Properties. *Crystals* **2023**, *13*, 612. <https://doi.org/10.3390/cryst13040612>

Academic Editors: Alessandra Toncelli and Željka Antić

Received: 28 February 2023

Revised: 19 March 2023

Accepted: 21 March 2023

Published: 3 April 2023



Copyright: © 2023 by the authors. Licensee MDPI, Basel, Switzerland. This article is an open access article distributed under the terms and conditions of the Creative Commons Attribution (CC BY) license (<https://creativecommons.org/licenses/by/4.0/>).

1. Introduction

In the region of northern Finland and Russia (NE Scandinavia), LCT (lithium–cesium–tantalum) pegmatites are exposed, containing lithium and columbite–tantalum mineralization [1]. In the case of Russia, this is the Kolmozero region, located in the northern part of the Kola Peninsula, where pegmatites up to several meters thick are exposed in the vicinity of Archean rocks [2–7]. In the case of Finland, it is in the Kaustinen region where such formations can be found [8,9]. These are rocks of granitoid composition, rich in quartz, plagioclase, and orthoclase, muscovite, and accessory minerals such as apatite and zircon. These minerals are accompanied by spodumene, and in its vicinity can be found several ore minerals, including grains of columbite–tantalite. These pegmatites are the product of residual crystallization under the influence of hydrothermal processes. The purpose of this article is to discuss the microscopic and spectroscopic differences between columbite–tantalite coming from these two regions.

2. Geology of the Study Area

The northern part of the Scandinavian Peninsula is part of the Baltic shield included in Fennoscandia [10–13] (Figure 1). It is a region located within Finland and Russia [14–16].

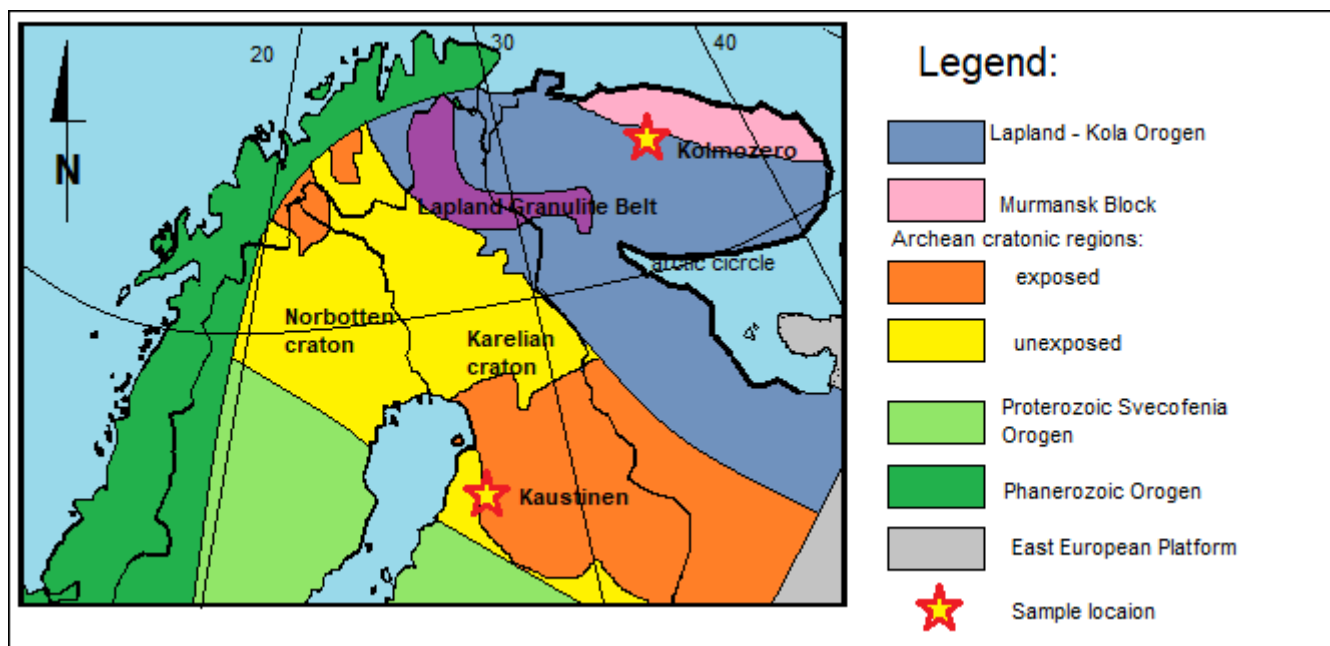


Figure 1. Simplified geological–tectonic map of the N Skandinavia (after [17]) with the samples' location.

Archean and Proterozoic gneisses metamorphosed in amphibolite and granulite facies are exposed there [18,19]. In these rocks, there are numerous younger intrusions with interesting mineralization [20]. Veins forming pegmatites mainly of granitoid composition are exposed there. Among these veins, LCT pegmatite are also encountered, characterized by spodumene/lepidolite–columbite–tantalite mineralization [21,22]. They usually form bodies of up to several meters in thickness, located over several tens of meters. In the Kolmozero area, these veins are located in the boundary zone between the Kola and Murmansk blocks, while in the Kaustinen area they accompany Belomorides (Figure 1). Their age has been estimated at 1.8–1.9 Ga years [23,24]. These rocks are exposed on the ground surface or covered by a small overburden of Pleistocene sediments [25,26]. These formations form an interesting landscape [27–31], with small hills and extended valleys with lots of lakes.

3. Materials and Methods

Rock samples were collected during numerous field investigations between 2018 and 2022. During this time, the discussed massifs were visited, and geological documentation of the samples was also collected. All the rock types investigated were collected in the Kolmozero and Kaustinen regions, from which only two representative samples from each area are presented in the paper. The selected rocks were targeted for thin section preparations to determine further the characteristics of the minerals discussed. Subsequently, these minerals were subjected to analyses using a Leica DM2500P polarizing optical microscope [32] and examination with a scanning electron microscope, the Hitachi SU6600, with an EDS (energy dispersive X-ray spectroscopy) attachment [33,34]. These samples were analyzed under low vacuum (10 Pa) with a 15 kV beam diameter of 0.2 μm . A total of 453 mineral analyses were performed in the microprobe (at Kaustinen 179 and Kolmozero 274, respectively). Next, the selected minerals were separated and analyzed with single-crystal X-ray diffraction. Data were collected on a Rigaku diffractometer (Rigaku, Tokyo, Japan) with $\text{CuK}\alpha$ radiation ($\lambda = 1.54184 \text{ \AA}$) at 293 K. Crystallographic refinement and data collection, as well as data reduction and analysis were performed with the CrysAlis^{Pro} v42 (Rigaku Oxford Diffraction, Tokyo, Japan) [35]. Selected single crystals were mounted on the nylon loop with oil. Structures were solved by applying direct methods using the SHELXS-86 program and refined with SHELXL–2018/3 [36–38] in Olex2 software [39]. Table 1 provides

the experimental details for the single crystal's X-ray measurement. These samples were also examined with the Raman technique [40,41]. Samples were measured using a Raman microscope in Via Reflex, Renishaw, UK. Optical and microscopic studies were performed in the Department of Geology, Soil Science, and Geoinformation of the Institute of Earth and Environmental Sciences, and crystal chemistry studies were performed at the Faculty of Chemistry.

Table 1. Single crystals X-ray diffraction results for all measured minerals.

Mineral	Columbite
Empirical formula	FeNb ₂ O ₆
Temperature/K	294
Crystal system	Orthorhombic
Space group	Pbcn
a/Å	14.281(2)
b/Å	5.7366(7)
c/Å	5.1234(5)
α/°	90
β/°	90
γ/°	90
Volume/Å ³	419.73(9)
Z	4
ρ _{calc} g/cm ³	5.344
Crystal size/mm ³	0.4 × 0.4 × 0.2
Data/restraints/parameters	361/0/17
Goodness-of-fit on F ²	2.703
Final R indexes [I > =2σ (I)]	R ₁ = 0.1743, wR ₂ = 0.5169
Largest diff. peak/hole/e Å ⁻³	41.40/−7.29

4. Results

The collected pegmatite samples were analyzed using the methods described above. Below are the results of these analyses.

4.1. Rocks Geology

4.1.1. Kaustinen

Exposed near Kaustinen, the pegmatites containing LCT mineralization coexist among biotite gneisses with magnetite [42]. Macroscopically, the pegmatites are cream-gray. They are characterized by a coarse crystalline structure, a compact texture, and disorder. Macroscopic observations show large, light gray plaques of plagioclase several cm in size, accompanied by greenish microcline. Next to these minerals, gray quartz and silvery mica are visible, forming small aggregates reaching up to 1 cm in size (Figure 2B). Next to these minerals is visible spodumene, whose size reaches several centimeters and is not inferior to plagioclase. In the microscopic image, the background of the rock is made up of quartz crystals sutured between each other, characterized by wavy extinction. They are accompanied by plaques of plagioclase and particle-rich, acidic albite, which form polysynthetic twinning. Next to these minerals, microcline can be found, also having an anhedral character similar to the other minerals mentioned. Between them, muscovite is seen in large numbers, forming variously oriented aggregates of lamellae (Figure 3C,D). Alongside these minerals, there are also small clusters of clinocllore. These minerals are accompanied by spodumene, which forms hypautomorphic crystals that often approximate each other. The crystals of this mineral are sometimes woven with fine muscovite and biotite. Muscovite is accompanied by epidote. Fine grains of zircon can be seen against the mica. Next to these minerals, fine ore crystals are visible, which are opaque. These minerals, along with epidote and fine muscovite, are also present on a background of microcline.



Figure 2. Macro photographs of the typical examples of LCT pegmatites from Kolmozero (A) and Kaustinen (B). Abbreviations: qtz—quartz, mu—muscovite, pl—plagioclase, sp—spodumene.

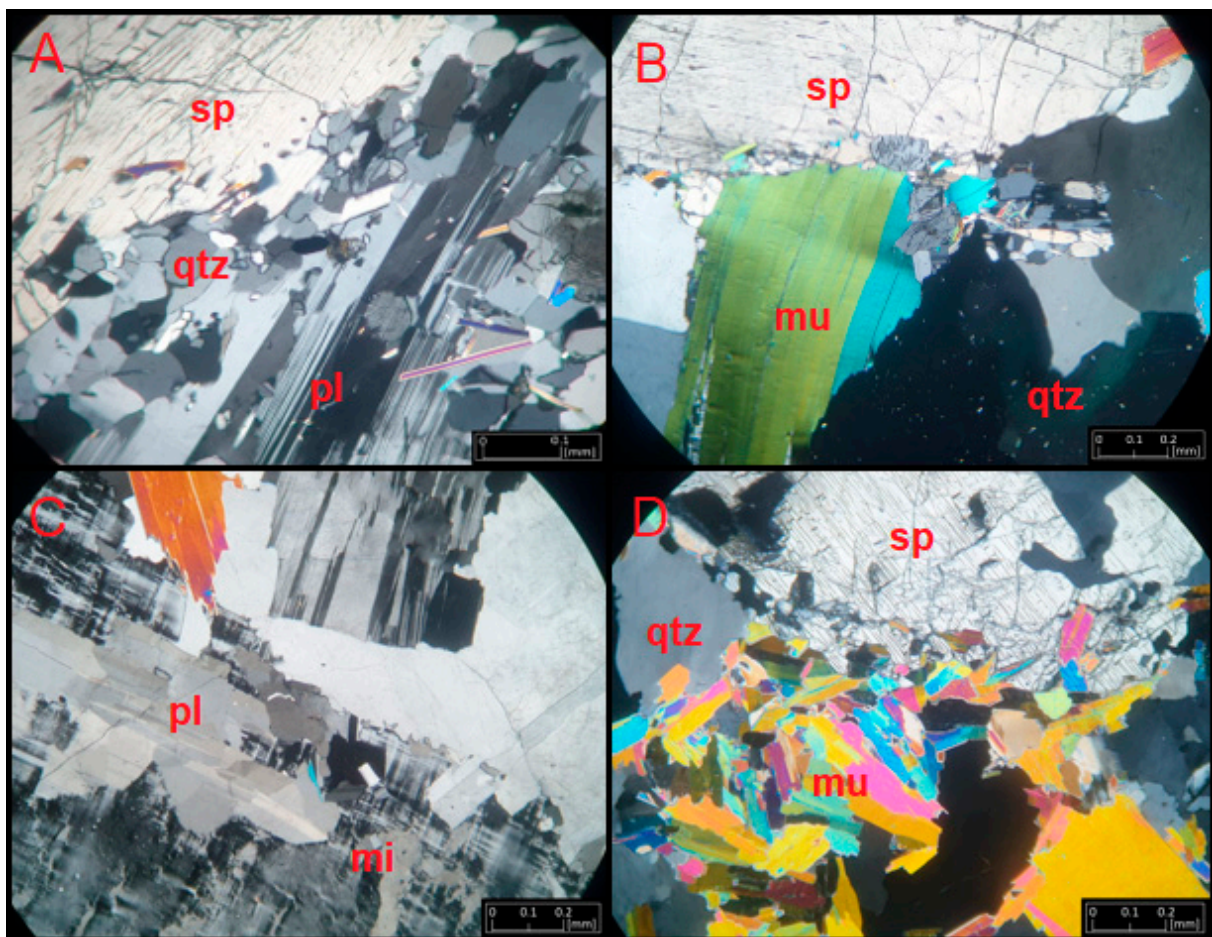


Figure 3. Microphotographs of the rocks from Kolmozero (A,B) and Kaustinen (C,D) with the typical association of the minerals and structures of rocks. There are present and microcline (mi), plagioclase (pl), quartz (qtz), muscovite (mu) and spodumene (sp).

4.1.2. Kolmozero

Among the gabbro-anorthosites that form a small intrusion in the Kolmozero belt are pegmatite bodies containing spodumene and lepidolite [43]. Macroscopically, they have a light cream-gray color. The presence of a coarse crystalline structure and a compact, disordered texture characterize them. On closer field observation, gray-cream plagioclase,

gray quartz, and accompanying large crystals of greenish-cream spodumene are visible (Figure 2A). Alongside these minerals, aggregates of muscovite and lepidolite are visible. Small-sized reddish garnets and bluish apatites can be seen as accessories. Accompanying columbite–tantalite minerals form black metallic inclusions among the rock-forming minerals. Microscopic images show large crystals of quartz, which form multi-grain clusters. These crystals have an anhedral shape and are in contact with each other (Figure 3A,B). Next to them, plagioclase is visible, represented mainly by an acidic variety, rich in albite particles. Usually, polysynthetic twinning forms small clusters of anhedral crystals between quartz grains. Alongside these minerals, microcline can be seen forming small crystals accompanied by quartz and plagioclase. These minerals are interspersed with scales of muscovite, which sometimes form significant aggregates. These minerals are sometimes deformed and disentangled; among them, quartz can be found usually in the form of small grains and small crystals of epidote. Small crystals of zircon and small crystals of garnet are present in the vicinity of mica. Small ore minerals are also visible, sometimes surrounded by goethite. Fine lamellae of muscovite can also be observed against some quartz grains. Small crystals of apatite can also be seen among the leucocratic minerals. Alongside these phases, large crystals of spodumene can be seen, which usually have a hypautomorphic shape. Spodumene in these rocks is usually approximated, co-occurring with muscovite and lepidolite. In those varieties of pegmatite where the amount of lepidolite is greater, spodumene usually forms relic corroded crystals interspersed with mica.

4.2. Results of SEM-EDS Analyses

The discussed crystals of columbite and tantalite form adhesions. The micro-area in the minerals shows the co-occurrence of these phases side by side. In these minerals, in addition to niobium (columbite) and tantalum (tantalite), there are variable admixtures of iron and manganese (Figures 4 and 5, Table A1). Tantalum in the minerals in question is an admixture oscillating between 11–20 wt% (see Table A1). Micro-area studies performed along the crystals in question showed that the ratio of iron to manganese and niobium to tantalum is variable throughout the crystal in both its central and edge parts. Most of these minerals have a significant admixture of niobium and a small proportion of tantalum. In the case of iron and manganese, these values are close to half (although with a predominance of manganese nitrogen). Due to the small size of the studied crystals in the samples in question and their strongly elongated shape, determining the changes in the proportions of these elements at the edge and center of these minerals is very difficult. In rocks from Kaustinen, it is accompanied by cassiterite, titanite, ilmenite, and magnetite in the form of small crystals. They coexist with galena, sphalerite, chalcopyrite, and barite. In the Kolmozero pegmatite, on the other hand, columbite–tantalite is accompanied by bixbyite, as well as clarkeite and selenite. Accompanying these minerals, quartz makes up a significant percentage of the rocks in question. Next to it is plagioclase, represented mainly by albite (84% of the crystals examined by SEM-EDS) with a small admixture of oligoclase (4%) and andesite-labradorite (6%). The pegmatites from Kaustinen also contain microcline, and the pegmatite from Kolmozero has orthoclase. In addition to these minerals, mica was found in the form of muscovite, co-mingling with spodumene and lepidolite. A small admixture of sodium (up to 5%) was found in muscovite. In addition, clinozoisite and epidote were found in pegmatites from Kaustinen. The accompanying spodumene contains a small admixture of sodium (averaging from less than 1% to 9%). Micro-area studies also made it possible to show that the coexisting phosphates are represented by a variety of hydroxyapatite, with about 3% carboxy apatite and 2% fluorapatite content.

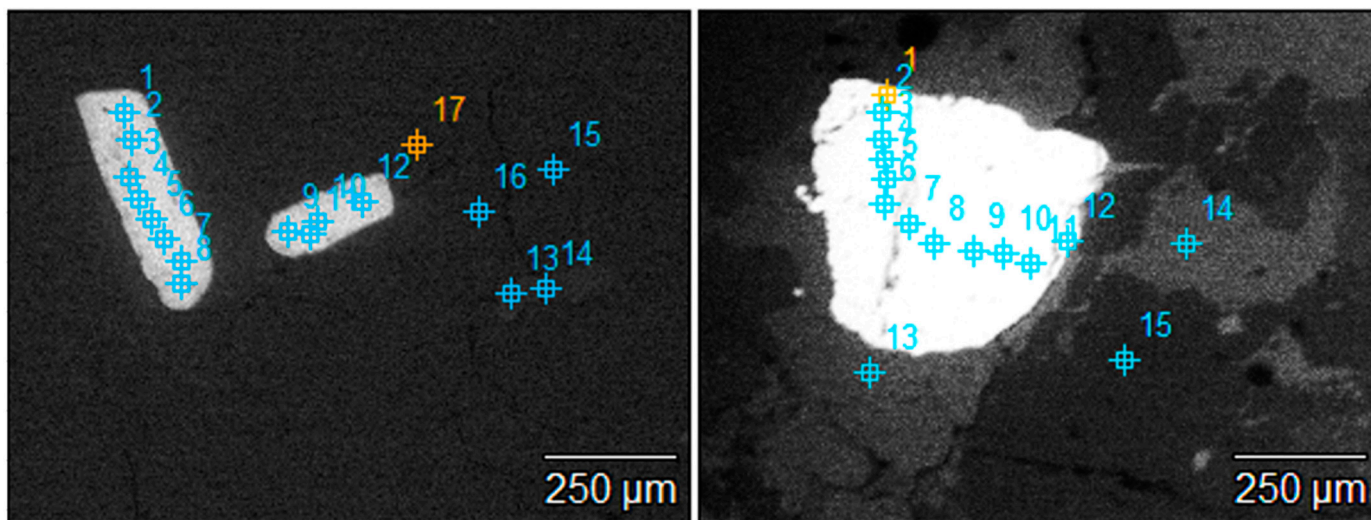


Figure 4. Backscattering electron microphotography of the columbite–tantalite grains with the marked analysis points.

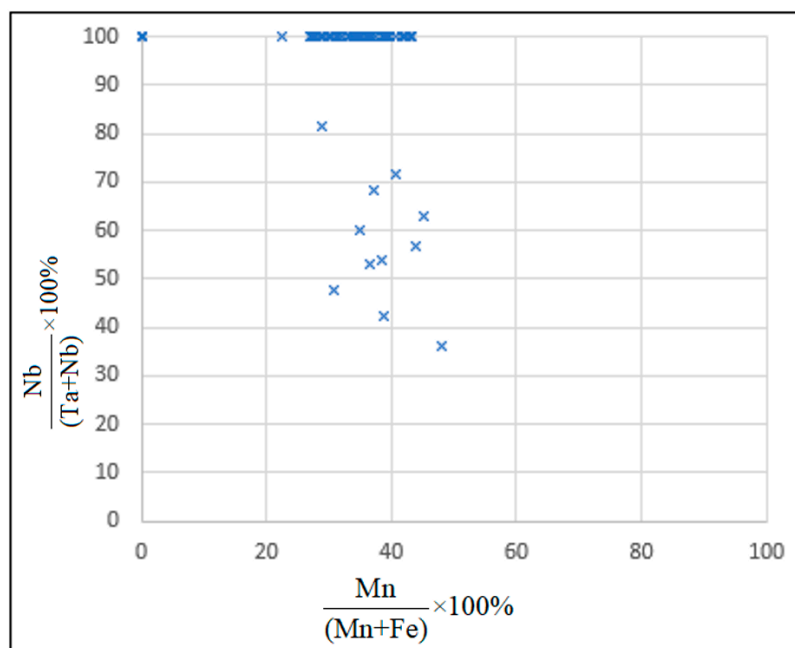


Figure 5. Proportion of the Fe, Mn, Nb, and Ta ions of the measured crystals.

4.3. Optical Properties of the Discussed Minerals

Macroscopically, crystals of columbite–tantalite have a black color with a metallic, rusty luster. They stand out from the minerals with which they coexist and are relatively easy to find. They have a size that reaches below 1 mm. Their quantity in Kolmozero pegmatites is much higher than that in Kaustinen, where this mineral is much rarer. In the microscopic image, Kolmozero tantalite crystals form small, jagged inclusions visible against a background of quartz and feldspar. In the case of rocks from Kolmozero, these crystals have a euhedral shape, forming much larger individuals visible against a background of spodumene and quartz. Rather, in the rocks from Kaustinen, it occurs in the form of single anhedral grains, sometimes of very elongated skeletal character. In the microscopic image, they are opaque black. In reflected light, this mineral has no clear relief and reflects light uniformly in a silvery gray color. In polarized light, the birefringence is barely visible due to the mineral's dark coloration (Figure 6).

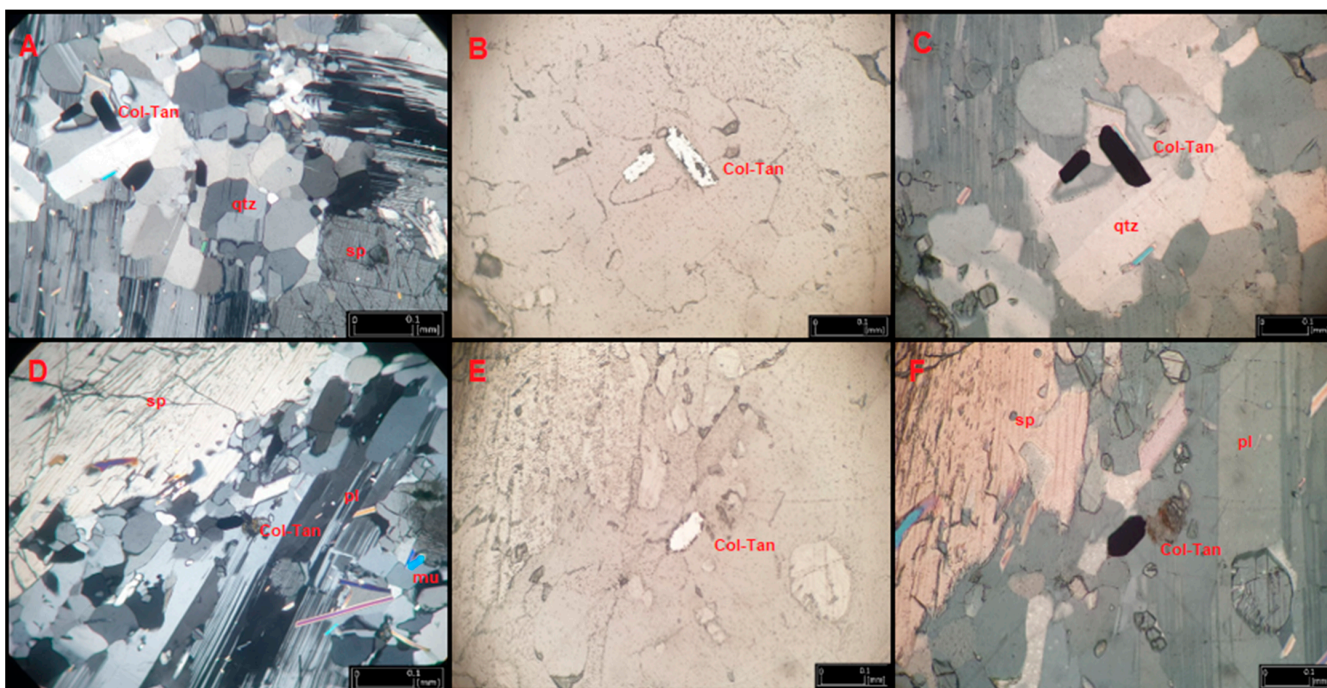


Figure 6. Images of columbite–tantalite (col-tan) in transmitted light (A,D) and reflected light (B,C,E,F), and under unpolarized light (B,E) and polarized light (A,C,D,F), showing the optical properties of this sample.

4.4. Spectroscopic Properties of the Discussed Minerals

Raman studies were conducted for a columbite–tantalite grain. Since it was a small grain, the spectrum shows only the most significant enhancements. The accompanying spectra show an enhancement in the region of 868 cm^{-1} , characteristic of Nb–O vibrations. Ca–O vibrations are noted at 793 cm^{-1} . The accompanying enhancement in the vicinity of 559 cm^{-1} corresponds to stretching vibrations for Nb–O. The observed vibration of 110 cm^{-1} corresponds to the stretching vibrations for Nb–Nb [44,45]. Some deviations from the standard spectra are due to the presence of manganese and iron admixtures in the minerals in question (Figure 7).

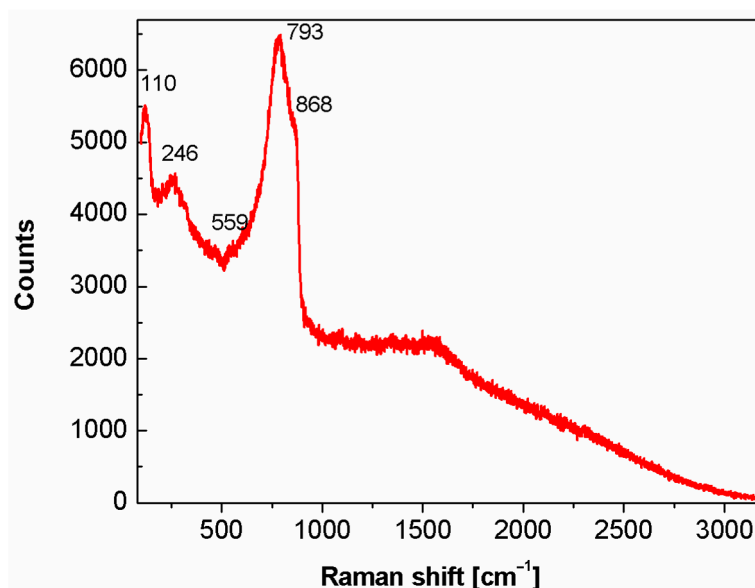


Figure 7. Raman spectrum for the columbite–tantalite crystals from Kolmozero.

4.5. Single Crystals Analysis Results

The examined crystal is a mixture of columbite–tantalite with iron and manganese substitution in varying proportions. These grains are present in the discussed pegmatites from both locations (Figure 8). The defecting of the crystals due to adhesions and fissures in this case made it difficult to determine their crystal structure. A presentation of this structure is given below [46]. Figure 8 presents the unit cell packing of the investigated columbite crystal. The relatively high R1 is related to low crystal quality. The solved structures indicate that the main building elements are Nb, Fe, and oxygen. However, the Fe position can be partly occupied by Mn, but the exact ratio between Fe and Mn was impossible to determine with this technique. Other elements are possible but in amounts smaller than 0.1 per atomic position. The unit cell parameters and space group are typical for this mineral and similar to those found by Boret et al. [47]. The Qiso parameters were set to 0.03 by hand to obtain the best fit of the model to the experimental data. As expected for this type of crystal with strong bonds, all the ATP values are smaller than 0.05 (see Tables A2–A5).

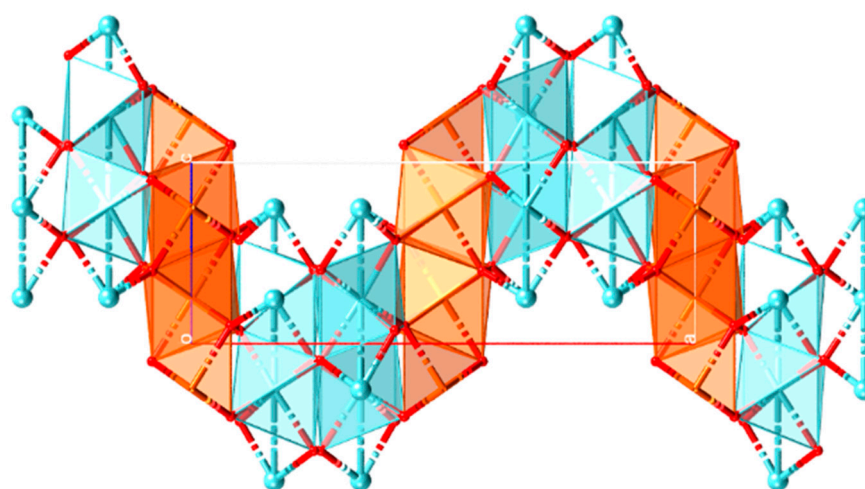


Figure 8. Crystal structure of columbite–tantalite (red line represents the *x*-axis and blue the *z*-axis).

5. Discussion

The discussed rocks containing columbite–tantalite mineralization are classified as granitoid pegmatites. These rocks are exposed in northern Scandinavia (in the area of the Kola Peninsula in Russia and the area of northern Finland) [48–51]. Although granitoid pegmatites in this area are visible in many places, further exploration of these rocks may increase the number of occurrences of LCT varieties. These rocks may be an interesting object of industrial exploration in the future, although their nature and the size of the observed exposures make such activities dependent on economic prosperity. An analysis of the mineralization of these pegmatites indicates that they represent the final stage of crystallization of residual melt, containing mismatched elements [52–56]. The presence of hydrated minerals in these rocks indicates that hydrothermal processes played a major role in the crystallization of minerals. This is also evidenced by sulfides and sulfates (barite, galena, sphalerite, and chalcopyrite). In addition, the chemical composition of ore minerals indicates the influence of fluids from the surrounding rocks [57]. This peculiarity is evident in the presence of such minerals including magnetite in the Kaustinen pegmatite and bismuth- and uranium-bearing minerals in the rocks at Kolomzero. Studies of niobium and tantalum minerals indicate that they form comagmatic adhesions that were formed during the same period of crystallization. Micro-area analyses have indicated both iron and manganese admixtures in both columbite and tantalite. In addition, there are variable amounts of niobium and tantalum in both minerals, which substitute for each other in the lattice. Additional difficulties such as cracks and close-ups prevented their separation

and thus hindered the analysis of the monocrystals by the X-ray method, showing their complex nature in the rocks in question. The analysis of the Raman spectrum obtained from these minerals is similar. The rocks in question are a solid solution in which the amount of iron and manganese varies according to the tests, as also shown by the analyses carried out along the grain from its boundary to the center of the grain.

6. Conclusions

Columbite–tantalite minerals are an important source of Nb and Ta. Their presence in LCT pegmatites, together with spodumene and lepidolite, is an interesting occurrence that may be the subject of further exploration in northern Scandinavia. These pegmatites represent a granitoid variety, crystallizing among Archean and Proterozoic rocks from the last portion of magma melt involving hydrothermal processes. Detailed studies of these minerals have shown their approximations, forming a solid solution. This means that these minerals were formed in one stage of crystallization.

Author Contributions: Conceptualization, M.H. and D.K.; methodology, M.H., D.K. and U.M.; validation, M.H., D.K. and U.M.; formal analysis, M.H.; investigation, resources, M.H.; data curation, M.H. and D.K.; writing—original draft preparation, M.H.; writing—review and editing, D.K.; visualization, M.H. and D.K.; All authors have read and agreed to the published version of the manuscript.

Funding: This research received no external funding.

Institutional Review Board Statement: Not applicable.

Informed Consent Statement: Not applicable.

Data Availability Statement: Not applicable.

Acknowledgments: The X-ray diffraction study was made possible with the support of EcoTech Complex in Lublin.

Conflicts of Interest: The authors declare no conflict of interest.

Appendix A

Table A1. SEM-EDS results of the columbite–tantalite crystals and modal composition of these phases based on the proportion of measure element.

Point	Elements Content [wt%]				Mineral	Modal Composition				
	O	Mn	Fe	Nb		Ta	Mn	Fe	Nb	Ta
Kolmozero(11)/1	26.20	15.97		29.59	Columbite	0.4	0.6	2.0	0.0	6
Kolmozero(11)/2	28.73	13.16		30.42	Columbite	0.3	0.7	2.0	0.0	6
Kolmozero(11)/3	28.52	12.60		29.13	Columbite	0.3	0.7	2.0	0.0	6
Kolmozero(11)/4	25.43	14.86	3.06	28.41	Columbite	0.3	0.7	2.0	0.0	6
Kolmozero(12)/1	24.05	17.31	3.64	29.53	Columbite	0.4	0.6	2.0	0.0	6
Kolmozero(12)/2	25.25	17.07	2.59	29.50	Columbite	0.4	0.6	2.0	0.0	6
Kolmozero(12)/3	31.42		2.87	35.90	Columbite	0.0	1.0	2.0	0.0	6
Kolmozero(12)/4	26.22	11.89	2.13	30.77	Columbite	0.3	0.7	2.0	0.0	6
Kolmozero(12)/5	26.71	11.55	4.82	30.76	Columbite	0.3	0.7	2.0	0.0	6
Kolmozero(12)/6	26.06	11.86	4.60	32.01	Columbite	0.3	0.7	2.0	0.0	6
Kolmozero(12)/7	24.67	13.25	6.32	30.86	Columbite	0.3	0.7	2.0	0.0	6
Kolmozero(12)/8	26.74	12.51	3.03	31.35	Columbite	0.3	0.7	2.0	0.0	6
Kolmozero(12)/10	24.74	17.61		30.98	Columbite	0.4	0.6	2.0	0.0	6
Kolmozero(12)/11	24.47	17.90	4.16	28.17	Columbite	0.4	0.6	2.0	0.0	6
Kolmozero(12)/12	24.47	15.22	4.50	30.48	Columbite	0.3	0.7	2.0	0.0	6
Kolmozero(26)/3	24.95	13.71		29.16	Columbite	0.3	0.7	2.0	0.0	6
Kolmozero(26)/4	22.18	16.45		31.93	Columbite	0.3	0.7	2.0	0.0	6
Kolmozero(26)/5	21.71	15.98	2.36	30.89	Columbite	0.3	0.7	2.0	0.0	6
Kolmozero(26)/6	22.58	13.00	2.89	32.18	Columbite	0.3	0.7	2.0	0.0	6
Kolmozero(26)/7	20.73	17.75	2.38	30.39	Columbite	0.4	0.6	2.0	0.0	6
Kolmozero(26)/8	23.32	12.29	8.60	28.03	Columbite	0.3	0.7	2.0	0.0	6

Table A1. Cont.

Point	Elements Content [wt%]				Ta	Mineral	Modal Composition				O
	O	Mn	Fe	Nb			Mn	Fe	Nb	Ta	
Kolmozero(26)/9	21.35	15.20	3.61	30.32		Columbite	0.3	0.7	2.0	0.0	6
Kolmozero(26)/10	21.56	16.23		32.44		Columbite	0.3	0.7	2.0	0.0	6
Kolmozero(26)/11	20.21	16.39	7.33	29.11		Columbite	0.4	0.6	2.0	0.0	6
Kolmozero(26)/12	22.39	12.44	4.36	32.02		Columbite	0.3	0.7	2.0	0.0	6
Kolmozero(26)/13	21.66	14.08	4.64	30.59		Columbite	0.3	0.7	2.0	0.0	6
Kolmozero(26)/14	22.86	15.71		31.96		Columbite	0.3	0.7	2.0	0.0	6
Kolmozero(26)/15	20.97	15.20	2.26	33.59		Columbite	0.3	0.7	2.0	0.0	6
Kolmozero(26)/16	29.96			7.98		Columbite	0.0	1.0	2.0	0.0	6
Kolmozero(30)/1	26.96	16.76		28.55		Columbite	0.4	0.6	2.0	0.0	6
Kolmozero(30)/2	27.87	17.17		27.47		Columbite	0.4	0.6	2.0	0.0	6
Kolmozero(30)/3	29.50	17.31		23.50		Columbite	0.4	0.6	2.0	0.0	6
Kolmozero(30)/4	29.74	13.11	0.52	28.69		Columbite	0.3	0.7	2.0	0.0	6
Kolmozero(30)/5	28.61	14.99	2.20	29.14		Columbite	0.3	0.7	2.0	0.0	6
Kolmozero(30)/6	35.06			33.87		Columbite	0.0	1.0	2.0	0.0	6
Kolmozero(30)/7	28.90	14.54	3.02	26.83		Columbite	0.4	0.6	2.0	0.0	6
Kolmozero(30)/8	29.19	14.36	1.81	27.75		Columbite	0.3	0.7	2.0	0.0	6
Kolmozero(30)/9	25.71	17.47	4.94	25.46		Columbite	0.4	0.6	2.0	0.0	6
Kolmozero(31)/1	40.06			18.81		Columbite	0.0	1.0	2.0	0.0	6
Kolmozero(34)/3	29.07	8.49	4.10	28.98		Columbite	0.2	0.8	2.0	0.0	6
Kolmozero(35)/1	28.25	14.79	3.06	25.94		Columbite	0.4	0.6	2.0	0.0	6
Kolmozero(35)/2	27.93	13.33	4.50	25.95		Columbite	0.3	0.7	2.0	0.0	6
Kolmozero(35)/3	28.01	14.39		27.27		Columbite	0.3	0.7	2.0	0.0	6
Kolmozero(35)/4	27.88	15.50	2.53	25.89		Columbite	0.4	0.6	2.0	0.0	6
Kolmozero(35)/5	27.54	16.15	2.04	24.85		Columbite	0.4	0.6	2.0	0.0	6
Kolmozero(35)/6	28.36	11.62	1.78	28.02		Columbite	0.3	0.7	2.0	0.0	6
Kolmozero(35)/7	26.24	16.35	3.23	25.40		Columbite	0.4	0.6	2.0	0.0	6
Kolmozero(35)/8	27.19	12.99	4.07	27.61		Columbite	0.3	0.7	2.0	0.0	6
Kolmozero(35)/9	27.16	14.95	3.46	26.32		Columbite	0.4	0.6	2.0	0.0	6
Kolmozero(35)/10	26.44	14.28	6.08	25.26		Columbite	0.4	0.6	2.0	0.0	6
Kolmozero(40)/1	24.59	16.55		29.23		Columbite	0.4	0.6	2.0	0.0	6
Kolmozero(40)/2	23.90	11.65	3.71	30.56		Columbite	0.3	0.7	2.0	0.0	6
Kolmozero(40)/3	24.04	14.89	4.28	28.26		Columbite	0.3	0.7	2.0	0.0	6
Kolmozero(40)/4	22.89	15.71		29.31		Columbite	0.3	0.7	2.0	0.0	6
Kolmozero(40)/5	25.31	12.72		29.89		Columbite	0.3	0.7	2.0	0.0	6
Kolmozero-2(1)/1	26.14	17.97	3.44	25.16		Columbite	0.4	0.6	2.0	0.0	6
Kolmozero-2(4)/1	24.83	22.65		30.17		Columbite	0.4	0.6	2.0	0.0	6
Kolmozero-2(4)/3	26.06	21.57	1.82	28.37		Columbite	0.4	0.6	2.0	0.0	6
Kaustinen-2(9)/1	29.86	13.02		23.37		Columbite	0.4	0.6	2.0	0.0	6
Kaustinen-2(9)/2	32.23	9.85	4.59	14.86		Columbite	0.4	0.6	2.0	0.0	6
Kaustinen-2(10)/1	34.57		3.18	21.38		Columbite	0.0	1.0	2.0	0.0	6
Kaustinen-2(10)/2	27.49	12.73	9.76	17.55		Columbite	0.4	0.6	2.0	0.0	6
Kaustinen-2(10)/10	33.17	5.45	1.84	10.43		Columbite	0.3	0.7	2.0	0.0	6
Kolmozero(12)/9	24.47	12.14	3.23	30.07	6.80	Tantalite	0.3	0.7	1.6	0.4	6
Kolmozero(30)/10	24.97	14.96	1.62	25.38	11.89	Tantalite	0.4	0.6	1.4	0.6	6
Kaustinen-2(10)/3	27.74	9.59	4.15	10.42	18.41	Tantalite	0.5	0.5	0.7	1.3	6
Kaustinen-2(10)/4	25.56	9.71	6.52	15.36	20.94	Tantalite	0.4	0.6	0.8	1.2	6
Kaustinen-2(10)/5	27.76	7.20	5.74	16.15	17.87	Tantalite	0.3	0.7	0.9	1.1	6
Kaustinen-2(10)/6	26.61	10.02	7.05	17.34	15.39	Tantalite	0.4	0.6	1.1	0.9	6
Kaustinen-2(10)/7	25.34	11.96	3.24	19.04	16.27	Tantalite	0.4	0.6	1.1	0.9	6
Kaustinen-2(10)/8	25.61	11.14	3.92	20.87	13.92	Tantalite	0.3	0.7	1.2	0.8	6
Kaustinen-2(10)/9	27.79	12.33	5.34	15.66	11.90	Tantalite	0.4	0.6	1.1	0.9	6
Kolmozero-2(4)/1	24.83	22.65		30.17		Columbite	0.4	0.6	2.0	0.0	6
Kolmozero-2(4)/2	20.54	21.86		31.72	12.52	Tantalite	0.4	0.6	1.4	0.6	6
Kolmozero-2(4)/3	26.06	21.57	1.82	28.37		Columbite	0.4	0.6	2.0	0.0	6
Kolmozero-2(4)/4	19.02	20.86	9.72	25.39	14.92	Tantalite	0.5	0.5	1.3	0.7	6

Appendix B

Table A2. Crystal data and structure refinement for Columbite_autored.

Identification Code	Columbite_Autored
Empirical formula	FeNb ₂ O ₆
Formula weight	337.67
Temperature/K	294
Crystal system	Orthorhombic
Space group	Pbcn
a/Å	14.281(2)
b/Å	5.7366(7)
c/Å	5.1234(5)
α/°	90
β/°	90
γ/°	90
Volume/Å ³	419.73(9)
Z	4
ρ _{calc} g/cm ³	5.344
μ/mm ⁻¹	70.926
F(000)	624.0
Crystal size/mm ³	0.4 × 0.4 × 0.2
Radiation	Cu Kα (λ = 1.54184)
2θ range for data collection/°	12.396 to 135.856
Index ranges	−15 ≤ h ≤ 16, −6 ≤ k ≤ 6, −5 ≤ l ≤ 6
Reflections collected	1425
Independent reflections	361 [R _{int} = 0.0351, R _{sigma} = 0.0211]
Data/restraints/parameters	361/0/17
Goodness-of-fit on F ²	2.703
Final R indexes [I >= 2σ (I)]	R ₁ = 0.1743, wR ₂ = 0.5169
Final R indexes [all data]	R ₁ = 0.1859, wR ₂ = 0.5396
Largest diff. peak/hole/e Å ⁻³	41.40/−7.29

Table A3. Fractional atomic coordinates (×10⁴) and equivalent isotropic displacement parameters (Å² × 10³) for Columbite_autored. U_{eq} is defined as 1/3 of the trace of the orthogonalized U_{ij} tensor.

Atom	x	y	z	U(eq)
Nb1	6641.6(14)	8256(6)	7555(3)	−1(2)
Fe1	5000	6716(12)	2500	−1(4)
O1	7568(14)	6200(30)	5910(40)	30
O3	5778(14)	3830(30)	4020(40)	30
O2	5961(15)	8960(30)	4280(40)	30

Table A4. Bond lengths for Columbite_autored.

Atom	Atom	Length/Å	Atom	Atom	Length/Å
Nb1	Nb1 ¹	3.250(4)	Fe1	O3	2.14(2)
Nb1	Nb1 ²	3.250(4)	Fe1	O3 ⁸	2.14(2)
Nb1	O1 ³	2.20(2)	Fe1	O2	2.09(2)
Nb1	O1 ⁴	2.08(2)	Fe1	O2 ⁸	2.09(2)
Nb1	O1	1.96(2)	O1	Nb1 ⁹	2.08(2)
Nb1	O3 ⁵	1.88(2)	O1	Nb1 ¹⁰	2.20(2)
Nb1	O2 ²	2.07(2)	O3	Nb1 ⁷	1.88(2)
Nb1	O2	1.98(2)	O3	Fe1 ⁶	2.13(2)
Fe1	O3 ⁶	2.13(2)	O2	Nb1 ¹	2.07(2)
Fe1	O3 ⁷	2.13(2)			

¹ +X, 2 − Y, −1/2 + Z; ² +X, 2 − Y, 1/2 + Z; ³ 3/2 − X, 1/2 + Y, +Z; ⁴ 3/2 − X, 3/2 − Y, 1/2 + Z; ⁵ +X, 1 − Y, 1/2 + Z; ⁶ 1 − X, 1 − Y, 1 − Z; ⁷ +X, 1 − Y, −1/2 + Z; ⁸ 1 − X, +Y, 1/2 − Z; ⁹ 3/2 − X, 3/2 − Y, −1/2 + Z; ¹⁰ 3/2 − X, −1/2 + Y, +Z.

Table A5. Bond angles for Columbite_autored.

Atom	Atom	Atom	Angle/°	Atom	Atom	Atom	Angle/°
Nb1 ¹	Nb1	Nb1 ²	104.03(18)	O2	Nb1	O1 ⁴	76.8(9)
O1 ³	Nb1	Nb1 ²	42.0(5)	O2	Nb1	O2 ²	88.5(7)
O1	Nb1	Nb1 ¹	91.8(6)	O3	Fe1	O3 ⁶	78.7(11)
O1	Nb1	Nb1 ²	135.1(6)	O3 ⁷	Fe1	O3 ⁸	162.9(11)
O1 ⁴	Nb1	Nb1 ²	80.2(6)	O3 ⁸	Fe1	O3 ⁶	85.3(7)
O1 ⁴	Nb1	Nb1 ¹	39.2(6)	O3 ⁷	Fe1	O3	85.3(7)
O1 ³	Nb1	Nb1 ¹	124.0(6)	O3 ⁷	Fe1	O3 ⁶	81.5(8)
O1	Nb1	O1 ⁴	87.2(5)	O3 ⁸	Fe1	O3	81.5(8)
O1	Nb1	O1 ³	94.6(5)	O2 ⁶	Fe1	O3	167.3(9)
O1 ³	Nb1	O1 ⁴	85.6(7)	O2	Fe1	O3 ⁷	96.6(7)
O1	Nb1	O2	95.1(8)	O2	Fe1	O3 ⁸	93.9(7)
O1	Nb1	O2 ²	164.7(10)	O2	Fe1	O3 ⁶	167.3(9)
O3 ⁵	Nb1	Nb1 ²	94.5(6)	O2 ⁶	Fe1	O3 ⁶	88.6(7)
O3 ⁵	Nb1	Nb1 ¹	135.1(7)	O2 ⁶	Fe1	O3 ⁸	96.6(7)
O3 ⁵	Nb1	O1	103.3(9)	O2	Fe1	O3	88.6(7)
O3 ⁵	Nb1	O1 ³	97.1(8)	O2 ⁶	Fe1	O3 ⁷	93.9(7)
O3 ⁵	Nb1	O1 ⁴	168.9(9)	O2 ⁶	Fe1	O2	104.0(11)
O3 ⁵	Nb1	O2 ²	90.8(8)	Nb1	O1	Nb1 ⁹	130.0(11)
O3 ⁵	Nb1	O2	98.4(8)	Nb1 ¹⁰	O1	Nb1 ⁹	98.8(8)
O2 ²	Nb1	Nb1 ²	35.7(6)	Nb1	O1	Nb1 ¹⁰	129.1(10)
O2	Nb1	Nb1 ²	122.8(6)	Nb1 ⁷	O3	Fe1 ⁸	125.7(10)
O2 ²	Nb1	Nb1 ¹	82.1(6)	Nb1 ⁷	O3	Fe1	133.7(11)
O2	Nb1	Nb1 ¹	37.5(6)	Fe1 ⁸	O3	Fe1	98.5(8)
O2 ²	Nb1	O1 ³	77.6(8)	Nb1	O2	Nb1 ¹	106.8(10)
O2	Nb1	O1 ³	159.4(8)	Nb1	O2	Fe1	124.5(10)
O2 ²	Nb1	O1 ⁴	79.2(9)	Nb1 ¹	O2	Fe1	126.7(10)

¹ +X, 2 − Y, −1/2 + Z; ² +X, 2 − Y, 1/2 + Z; ³ 3/2 − X, 1/2 + Y, +Z; ⁴ 3/2 − X, 3/2 − Y, 1/2 + Z; ⁵ +X, 1 − Y, 1/2 + Z; ⁶ 1 − X, 1 − Y, 1 − Z; ⁷ +X, 1 − Y, −1/2 + Z; ⁸ 1 − X, +Y, 1/2 − Z; ⁹ 3/2 − X, 3/2 − Y, −1/2 + Z; ¹⁰ 3/2 − X, −1/2 + Y, +Z.

References

- Lahtinen, R.; Garde, A.A.; Melezhik, V.A. Paleoproterozoic evolution of Fennoscandia and Greenland. *Episodes* **2008**, *31*, 20–28. [[CrossRef](#)] [[PubMed](#)]
- Bayanova, T.B.; Kunakkuzin, E.L.; Serov, P.A.; Steshenko, E.; Borisenko, E.S.; Turkina, O. The Oldest Grey Gneisses and Tonalite-Ironhjemetite Granodiorites in the Fennoscandian Shield: ID-TIMS and SHRIMP Data. *Open J. Geol.* **2020**, *10*, 124–136. [[CrossRef](#)]
- Bibikova, E.V.; Bogdanova, S.V.; Postnikov, A.V.; Popova, L.P.; Kirnozova, T.I.; Fugzan, M.M.; Glushchenko, V.V. Sarmatia–Volgo-Uralia Junction Zone: Isotopic–Geochronologic Characteristic of Supracrustal Rocks and Granitoids. *Stratigr. Geol. Correl.* **2009**, *17*, 561–573. [[CrossRef](#)]
- Andersson, J.; Möller, C.; Johansson, L. Zircon geochronology of migmatite gneisses along the Mylonite Zone (S Sweden): A major Sveconorwegian terrane boundary in the Baltic shield. *Precambrian Res.* **2002**, *114*, 14–121. [[CrossRef](#)]
- Glebovitsky, V.A. *Early Precambrian of the Baltic Shield*; Nauka: St. Petersburg, Russia, 2005; p. 710. (In Russian)
- Pozhilienko, V.I.; Gavrilenko, B.V.; Zhironov, C.V.; Zhabin, S.V. *Geology of Mineral Areas of the Murmansk Region*; Kola Scientific Center, Russian Academy of Sciences: Moscow, Russia, 2002; p. 360. (In Russian)
- Bridgewater, D.; Scott, D.J.; Balagansky, V.V.; Timmerman, M.J.; Marker, M.; Bushmin, A.; Alexeyev, N.L.; Daly, J.S. Age and Provenance of Early Precambrian Metasedimentary Rocks in the Lapland-Kola Belt, Russia: Evidence from Pb and Nd Isotopic Data. *Terra Nova* **2001**, *13*, 32–37. [[CrossRef](#)]
- Hölttä, P.; Heilimo, E.; Huhma, H.; Juopperi, H.; Kontinen, A.; Konnunaho, H.; Lauri, L.; Mikkola, P.; Paavola, J.; Sorjonen-Ward, P. Archaean Complexes of the Karelia Province in Finland. *Geol. Surv. Finl. Spec. Pap.* **2012**, *54*, 9–20.
- Timmerman, M.J.; Daly, S.J. Sm-Nd Evidence for Late Archaean Crust Formation in the Lapland-Kola Mobile Belt, Kola Peninsula, Russia and Norway. *Precambrian Res.* **1995**, *72*, 97–107. [[CrossRef](#)]
- Huber, M.; Bayanova, T.B.; Serov, P.A.; Skupiński, S. *Archaean Gneisses of the Murmansk, Oleniegorsk Region, NE Fennoscandia, in the Light of the Petrographic and Geochemical Analysis*; Sciences Publisher: Lublin, Poland, 2018; p. 181. (In Polish)
- Hałas, S.; Huber, M.; Piętrzyński, A. Petrology of gabbroides and isotope signature of sulfide mineralization from Fedorov-Pansky layered mafic intrusion, Kola peninsula, Russia. *Geochronometria* **2009**, *33*, 19–22. [[CrossRef](#)]

12. Huber, M.A.; Hałas, S.; Neradovsky, Y.N.; Bayanova, T.B.; Mokrushin, A.W.; Lata, L. Stable isotope geochemistry of sulfides from intrusion in Monchegorsk, Northern part of Baltic shield. *Geochronometria* **2016**, *43*, 96–101. [[CrossRef](#)]
13. Huber, M.; Stepniowska, K. Application of the Fractal Dimension Calculation Technique to Determine the Shape of Selected Monchepluton Intrusion Crystals (NE Fennoscandia). *Minerals* **2021**, *11*, 1140. [[CrossRef](#)]
14. Torske, T.; Bergh, S. The Caravari Formation of the Kautokeino Greenstone Belt, Finnmark, North Norway, a Palaeoproterozoic foreland basin succession. *NG U-BU LL* **2004**, *442*, 5–22.
15. Bingen, B.; Solli, A.; Viola, G.; Torgersen, E.; Sandstad, J.S.; Whitehouse, M.J.; Nasuti, A.; Røhr, T.R.; Ganerød, M.; Nasuti, A. Geochronology of the Palaeoproterozoic Kautokeino Greenstone Belt, Finnmark, Norway: Tectonic implications in a Fennoscandia context. *Nor. J. Geol.* **2015**, *95*, 365–396. [[CrossRef](#)]
16. Henderson, I.H.; Viola, G.; Nasuti, A. A new tectonic model for the Palaeoproterozoic Kautokeino Greenstone Belt, northern Norway, based on high-resolution airborne magnetic data and field structural analysis and implications for mineral potential. *Nor. J. Geol.* **2015**, *95*, 339–363. [[CrossRef](#)]
17. Smith, E.; Wang, W. Diamond with Concentric Inclusions. *Gems Gemol.* **2017**, *53*, 228–239.
18. Petrovskaya, L.S.; Mitrofanov, F.P.; Bayanova, T.B.; Petrov, V.P.; Petrovski, M.N. *Neoarchean Enderbites-Granulite Complex of the Pulozero-Polnek-Tundra Region, Central Kola Block: Stages and the Thermodynamic Regime of Evolution*; Kola Science Centre RAS: Kola Peninsula, Russia, 2010; p. 78. (In Russian)
19. Petrovskaya, L.S.; Mitrofanov, F.P.; Bayanova, T.B.; Serov, P.A. The Archean Pulozero–Polnek–Tundra Enderbite–Granulite Complex of the Central Kola Block: Stages and Formation Conditions (Kola Peninsula). *Dokl. Akad. Nauk.* **2007**, *416*, 370–373. [[CrossRef](#)]
20. Huber, M.; Kamiński, D.; Czernel, G.; Kozlov, E. Optical and Spectroscopic Properties of Lorenzenite, Loparite, Perovskite, Titanite, Apatite, Carbonates from the Khibiny, Lovozero, Kovdor, and Afrikanda Alkaline Intrusion of Kola Peninsula (NE Fennoscandia). *Crystals* **2022**, *12*, 224. [[CrossRef](#)]
21. Morozova, L.N. Rare-metal pegmatites of the Soldat-Myl'k pegmatite field: Geology, geochemistry of rare elements. In IOP Conference Series: Earth and Environmental. *Science* **2020**, *539*, 012162. [[CrossRef](#)]
22. Morozova, L.N.; Sokolova, E.N.; Smirnov, S.Z.; Balagansky, V.V.; Bazai, A.V. Spodumene from rare-metal pegmatites of the Kolmozero lithium world-class deposit on the Fennoscandian shield: Trace elements and crystal-rich fluid inclusions. *Mineral. Mag.* **2021**, *85*, 149–160. [[CrossRef](#)]
23. Al-Ani, T.; Ahtola, T. Mineralogy of spodumene pegmatites, Kaustinen, Western Finland. *Geol. Surv. Finl. Rep. M* **2008**, *19*, 1–48.
24. Morozova, L.N. The Kolmozero lithium deposit of rare metal pegmatites: New data on the rare element composition (Kola Peninsula). *Lithosphere* **2018**, *18*, 82–98. [[CrossRef](#)]
25. Evzerov, V.Y. Glacier Deposits As Unique Formations in the Loose Cover of the Baltic Shield. *Lithol. Miner. Resour.* **2001**, *36*, 109–115. [[CrossRef](#)]
26. Korsakova, O.P. Pleistocene marine deposits in the coastal areas of Kola Peninsula (Russia). *Quat. Int.* **2009**, *206*, 3–15. [[CrossRef](#)]
27. Huber, M.; Rusek, A.; Menshakova, M.; Zhigunova, G.; Chmiel, S.; Iakovleva, O. Possibilities of Sustainable Development including Improvement in Air Quality for the City of Murmansk-Examples of Best Practice from Scandinavia. *Climate* **2022**, *10*, 15. [[CrossRef](#)]
28. Huber, M.; Iakovleva, O. Tourism, Scientific, and Didactic Potential of the Ultrabasic-Alkaline Intrusion in Afrikanda with Perovskite Mineral (Kola Peninsula, N Russia) and of the Related Built Heritage. *Heritage* **2021**, *4*, 3892–3907. [[CrossRef](#)]
29. Huber, M.; Zhigunova, G.; Menshakova, M.; Iakovleva, O.; Karimova, M. Geoheritage of the Monchegorsk Igneous Layered Paleoproterozoic Intrusion (Kola Peninsula, Arctic Russia): Evaluation and Geotourism Opportunities. *Heritage* **2021**, *4*, 3583–3610. [[CrossRef](#)]
30. Huber, M.; Zhigunova, G.; Menshakova, M.; Gainanova, R.; Iakovleva, O. Geoheritage of the Kandalaksha region (Kola Peninsula, White Sea, Arctic Russia), Evaluation, and Geotourism Opportunities. *Geoheritage* **2022**, *14*, 112. [[CrossRef](#)]
31. Huber, M.; Iakovleva, O.; Zhigunova, G.; Menshakova, M.; Gainanova, R. Can the Arctic be saved for the next generations? Study of examples and internships in Murmansk District. *IOP Conf. Ser. Earth Environ. Sci.* **2021**, *678*, 01203. [[CrossRef](#)]
32. Bowers, D.G.; Binding, C.E. The optical properties of mineral suspended particles: A review and synthesis. *Estuar. Coast. Shelf Sci.* **2006**, *67*, 219–230. [[CrossRef](#)]
33. Gu, Y. Automated scanning electron microscope based mineral liberation analysis. *J. Miner. Mater. Charact. Eng.* **2003**, *2*, 33–41.
34. Pirrie, D.; Power, M.R.; Rollinson, G.K.; Wiltshire, P.E.; Newberry, J.; Campbell, H.E. Automated SEM-EDS (QEMSCAN[®]) mineral analysis in forensic soil investigations: Testing instrumental reproducibility. *Crim. Environ. Soil Forensics* **2009**, 411–430.
35. Rigaku. *CRYSTALIS Software System*; Rigaku: Oxford, UK, 2016.
36. Sheldrick, G.M. SHELXT—Integrated space-group and crystal-structure determination. *Acta Crystallogr.* **2015**, *A71*, 3–8. [[CrossRef](#)] [[PubMed](#)]
37. Sheldrick, G.M. A short history of SHELX. *Acta Crystallogr.* **2008**, *A64*, 112–122. [[CrossRef](#)]
38. Sheldrick, G.M. Crystal structure refinement with SHELXL. *Acta Crystallogr.* **2015**, *C71*, 3–8.
39. Dolomanov, O.V.; Bourhis, L.J.; Gildea, R.J.; Howard, J.A.K.; Puschmann, H.J. A Complete Structure Solution, Refinement and Analysis Program. *Appl. Cryst.* **2009**, *42*, 339–341. [[CrossRef](#)]
40. Amarie, S.; Zaslansky, P.; Kajihara, Y.; Griesshaber, E.; Schmahl, W.W.; Keilmann, F. Nano-FTIR chemical mapping of minerals in biological materials. *Beilstein J. Nanotechnol.* **2012**, *3*, 312–323. [[CrossRef](#)] [[PubMed](#)]

41. Pleshko, N.; Boskey, A.; Mendelsohn, R. Novel infrared spectroscopic method for the determination of crystallinity of hydroxyapatite minerals. *Biophys. J.* **1991**, *60*, 786–793. [[CrossRef](#)]
42. Steiner, B.M. Tools and workflows for grassroots Li–Cs–Ta (LCT) pegmatite exploration. *Minerals* **2019**, *9*, 499. [[CrossRef](#)]
43. Vrevskii, A.B. Age and sources of the anorthosites of the Neoproterozoic Kolmozero-Voron'ya greenstone belt (Fennoscandian Shield). *Petrology* **2016**, *24*, 527–542. [[CrossRef](#)]
44. Beskin, S.M.; Marin, Y.B. Comprehensive systematics of tantalum and tantalum-niobium deposits. *Geol. Ore Depos.* **2016**, *58*, 536–541. [[CrossRef](#)]
45. Husson, E.; Repelin, Y.; Dao, N.Q.; Brusset, H. Normal coordinate analysis for CaNb_2O_6 of columbite structure. *J. Chem. Phys.* **1977**, *66*, 5173. [[CrossRef](#)]
46. Yang, H.; Zhang, S.; Yang, H.; Yuan, Y.; Li, E. Intrinsic dielectric properties of columbite ZnNb_2O_6 ceramics studied by P–V–L bond theory and Infrared spectroscopy. *J. Am. Ceram. Soc.* **2019**, *102*, 5365–5374. [[CrossRef](#)]
47. Bordet, P.; McHale, A.; Santoro, A.; Roth, R.S. Powder neutron diffraction study of ZrTiO_4 , $\text{Zr}_5\text{Ti}_7\text{O}_{24}$, and FeNb_2O_6 . *J. Solid State Chem.* **1986**, *64*, 30–46. [[CrossRef](#)]
48. Pripachkin, P.V.; Kudryashov, N.M.; Rundkvist, T.V.; Morozova, L.N. Lithium in pegmatites of the Fennoscandian Shield and operation prospects for the Kolmozero deposit on the Kola Peninsula (Russia). *Appl. Earth Sci.* **2022**, *131*, 179–192. [[CrossRef](#)]
49. Gordienko, V.V.; Gordienko, V.V.; Sergeev, A.S.; Levskii, L.K.; Lokhov, K.I.; Kapitonov, I.N.; Sergeev, S.A. First data in favor of the crystallization model of lithium isotope fractionation in the pegmatitic process. *Dokl. Earth Sci.* **2007**, *413*, 441. [[CrossRef](#)]
50. Mueller, M.; Peltonen, P.; Eilu, P.; Goldfarb, R.; Hanski, E. The Mustajärvi orogenic gold occurrence, Central Lapland Greenstone Belt, Finland: A telluride-dominant mineral system. *Miner. Depos.* **2020**, *55*, 1625–1646. [[CrossRef](#)]
51. Kudryashov, N.M.; Petrovsky, M.N.; Mokrushin, A.V.; Elizarov, D.V. Neoproterozoic sanukitoid magmatism in the Kola region: Geological, petrochemical, geochronological, and isotopic-geochemical data. *Petrology* **2013**, *21*, 351–374. [[CrossRef](#)]
52. Maxwell, P.; Mora, M. Lithium and Chile: Looking back and looking forward. *Miner. Econ.* **2020**, *33*, 57–71. [[CrossRef](#)]
53. Beskin, S.M.; Marin, Y.B. Granite systems with rare-metal pegmatites. *Geol. Ore Depos.* **2020**, *62*, 554–563. [[CrossRef](#)]
54. El-Enen, M.A.; Okrusch, M.; Will, T.M. Metapelitic assemblages in the Umm Zariq schists, central western Kid belt, Sinai Peninsula, Egypt. *Neues Jahrb. Fur Mineralogie. Abh.* **2003**, *178*, 277–306. [[CrossRef](#)]
55. Černý, P.; London, D.; Novák, M. Granitic pegmatites as reflections of their sources. *Elements* **2012**, *8*, 289–294. [[CrossRef](#)]
56. Bradley, D.C.; McCauley, A.A. *Preliminary Deposit Model for Lithium-Cesium-Tantalum (LCT) Pegmatites*; US Geological Survey: Washington, DC, USA, 2013. [[CrossRef](#)]
57. Sami, M.; El Monsef, M.A.; Abart, R.; Toksoy-Köksal, F.; Abdelfadil, K.M. Unraveling the Genesis of Highly Fractionated Rare-Metal Granites in the Nubian Shield via the Rare-Earth Elements Tetrad Effect, Sr–Nd Isotope Systematics, and Mineral Chemistry. *ACS Earth Space Chem.* **2022**, *6*, 2368–2384. [[CrossRef](#)]

Disclaimer/Publisher's Note: The statements, opinions and data contained in all publications are solely those of the individual author(s) and contributor(s) and not of MDPI and/or the editor(s). MDPI and/or the editor(s) disclaim responsibility for any injury to people or property resulting from any ideas, methods, instructions or products referred to in the content.